Eng. Sci., 2025, **37**, 1738

Engineered Science
DOI: https://dx.doi.org/10.30919/es1738

# Construction of Cyano-modified Ultrathin Graphitic Carbon Nitride for Boosted Photocatalytic Degradation of High Concentration Tetracycline

Xijue Tang, Huanhuan Zhai,* Wenqiang Luo, Guoyong Wang, Shaohui Xiong, Hongwei Zhao, Xinxiu Cao, Danyu Zhang and Qingquan Liu*

## Abstract

Photocatalytic degradation of tetracycline has received widespread attention as a green wastewater treatment technology. However, the current degradation efficiency is still limited by the insufficient oxidation ability and high recombination efficiency of photo-generated carriers. In this research, cyano-modified ultrathin graphitic carbon nitride (g-$C_3N_4$) is synthesized by a facile salt-assisted heat treatment method. As a result, it displays a satisfactory photo-degradation efficiency of 98.96% in 60 min, particularly for the high concentration tetracycline of 100 mg $L^{-1}$. The underlying causes lie in the cyano groups, which act as electron trapping groups, effectively suppress the recombination of charge carriers. Meanwhile, the ultrathin nanosheet structure of g-$C_3N_4$ validly augments the active sites on the surface, as well as shortens the carriers migrating route. The synergistic effect of the above optimizes the carrier migration kinetics of g-$C_3N_4$, thus achieving superior photocatalytic degradation performance. This study paves the way for the extensive application of g-$C_3N_4$ in photocatalytic wastewater treatment technology and offers promising prospects for its future development.

*Keywords:* Photocatalysis; g-$C_3N_4$; Tetracycline degradation; Cyano groups; Ultrathin nanosheet structure.
Received: 09 May 2025; Revised: 22 July 2025; Accepted: 06 August 2025
Article type: Research article.

## 1.Introduction

Tetracycline (TC), a common antibiotic, is frequently employed in the treatment of diverse bacterial infections.[1] However, TC has become a serious threat to the environment due to its excessive use and weak self-degradation ability.[2] As an effective method for wastewater treatment, photocatalytic technology exhibits great potential to replace traditional chemical treatment methods due to its high efficiency, environmental protection, and low cost. Among a series of reported photocatalysts, graphitic carbon nitride (g-$C_3N_4$), as a novel semiconductor photocatalyst for nonmetallic compounds, has received much attention in the field of photocatalysis owning to its excellent thermal-chemical and photo-chemical stability.[3] However, its photocatalytic efficiency in application is still limited by the shortcomings of insufficient specific surface area, confined visible light absorption range, and high photogenerated carrier recombination rate.[4-5] Hence, there is an urgent need to develop new modification strategies to further improve the catalytic activity of g-$C_3N_4$.

At present, a diverse array of modification methods are being implemented on g-$C_3N_4$, such as morphological modulation,[6-7] elemental doping,[8-9] vacancy defects,[10] and heterostructure construction.[11-13] Among them, the functional group modification mainly enhances the photocatalytic performance of g-$C_3N_4$ by improving the energy band structure.[14] Cheng *et al*. has reported that metal-free phenyl groups are grafted onto the edge of g-$C_3N_4$ by using 4-phenyl-3-thiosemicarbazide and urea as precursors. The edge modification and energy level improving are realized by one-step copolymerization. As a result, the optimal photocatalytic hydrogen production rate of the modified g-$C_3N_4$ reaches 2390.6 μmol $h^{-1}g^{-1}$, and the apparent quantum efficiency (AQE) at 420 nm reaches 8.3%.[15] Zhou *et al*. has prepared g-$C_3N_4$

*School of Material Science and Engineering, Hunan Provincial Key Laboratory of Advanced Materials for New Energy Storage and Conversion, Hunan University of Science and Technology, Xiangtan, Hunan, 411201, China*
**Email:* zhaihh@hnust.edu.cn (Huanhuan Zhai), qqliu@hnust.edu.cn (Qingquan Liu)

with a porous thin-layer structure through the gas templating method, using thiourea as a precursor and ammonium chloride as a sacrificial agent. This process adjusts the energy band structure and enhances the electron reduction ability. As a result, the degradation efficiency of the product increases from 68% to 92%, and the kinetic constant of phenol degradation is four times higher than that of pristine g-$C_3N_4$.[16]

Morphological modulation is an effective strategy to improve the photocatalytic performance of g-$C_3N_4$ by shortening the carrier transport path and providing more active sites.[17] The team modified the morphology of g-$C_3N_4$ in the g- g-$C_3N_4$-Pt photocatalyst using a simple hydrothermal method and investigated its effect on hydrogen evolution performance. Prolonged hydrothermal treatment altered the morphology of g-$C_3N_4$, creating more oxygen-containing functional groups at the edges of expanded melem unit defects, resulting in a hydrogen yield of 151.4 mmol·$g_{Pt}^{-1}$.[18] The Zheng team used melamine-cyanuric acid supramolecular (MCS) precursors to prepare CN/$Mn_2O_3$/FTO p-n heterojunctions on FTO substrates, which remained intact after five cycles of PEC testing, indicating structural stability and excellent mechanical strength.[19] Either functional group modification or morphological regulation can enhance the utilization efficiency of charge carriers. However, the optimization of catalytic reaction kinetics remains a pivotal focus in the current field of photocatalytic degradation. Therefore, the approach of synergistic modification through multiple strategies is a necessary means to enhance the catalytic reaction kinetics of g-$C_3N_4$ and expand its development space in the field of pollutant degradation.

In this paper, cyano-modified ultrathin g-$C_3N_4$ are synthesized by a facile salt-assisted heat treatment method. The experimental results showed that the photodegradation efficiency of high concentration of TC (concentration of 100 mg/L) reached 98.96% with the degradation rate constant k value as high as 0.04936 $min^{-1}$ after the light duration of 60 min. The performance enhancement is attributed to the ultrathin nanosheet structure of g-$C_3N_4$ that effectively increases the active sites on the surface while reducing the carrier migration path. Furthermore, as an electron-withdrawing group, cyano can effectively suppress the combination efficiency of charge carriers. Thus, the synergistic effect of the ultrathin structure and cyano groups effectively improves the photocatalytic reaction kinetics. Our research advocates green technology as an alternative to traditional processes, which meets the goal of "carbon neutrality" and provides a sustainable technology pathway for wastewater treatment in the pharmaceutical and aquaculture industries.[20]

## 2. Experimental procedure

### 2.1 Synthesis of g-$C_3N_4$ samples

First, 4 g of dicyandiamide and 100 mL of water were added to a container and sonicated for 10 min, followed by the addition of 6 g, 8 g, 10 g, 12 g, or 14 g of NaCl, which was sonicated until it was completely dissolved. Then the solution was quickly frozen with liquid nitrogen, and then placed in a freeze dryer for drying. Subsequently, the dried powder was transferred to a corundum beaker and calcined at 550 ℃ for 4 h at a rate of 2.3 ℃/min under an atmosphere of $N_2$. After natural cooling, the powder was ground, cleaned, and then dried in vacuum at 60 ℃ for 12 h. The series of cyano-modified ultrathin g-$C_3N_4$ obtained were named as cyano-UCN 4:6, cyano-UCN 4:8, cyano-UCN 4:10, cyano-UCN 4:12, and cyano-UCN 4:14, respectively in related with the ratio of dicyandiamide and NaCl. Its comparative sample (CN) was synthesized without the addition of NaCl, and the rest of the steps were consistent with the synthesis of cyano-UCN.

### 2.2 Characterization

Fourier transform infrared (FT-IR) spectra were obtained using a Nicolet iS 10 spectrometer. X-ray photoelectron spectroscopy (XPS) analysis was obtained with an ESCALAB 250Xi spectrometer. X-ray diffraction spectroscopy (XRD) was used to obtain the crystal structure of the material with a Bruke D8 Advance diffractometer equipped with Cu Kα radiation. The transmission electron microscope (TEM) was conduct by using FEI Tecnai F20. Specific surface area analysis (BET) was obtained using a TriStar II Plus 3Flex gas adsorption analyzer. Solid-state UV-Vis diffuse reflectance spectra (DRS) were obtained at room temperature using a PE lambda 750 spectrophotometer. Photoluminescence (PL) spectra of g-$C_3N_4$ were obtained by an Edinburgh FLS 980 spectrophotometer. Time-resolved luminescence spectra (TRPL) of the samples were analyzed with an Aerospace FLS1000 fluorescence lifetime spectrophotometer. CHI660E electrochemical workstation and standard three-electrode system (working electrode, Pt electrode and Ag/AgCl reference electrode) were selected for the photoelechemical performance, and the solution was 0.5 M $Na_2SO_4$. Electron Spin Resonance (ESR) were performed by using a Bruker EMXplus, and the liquid chromatography-mass spectrometer (LC-MS) was detected by Thermo Fisher Ultimate 3000 UHPLC-Q Exactive.

### 2.3 Photocatalytic degradation performance

The photocatalytic degradation of TC by the g-$C_3N_4$ sample was investigated to assess its activity under visible light irradiation. The light source was provided by a 300 W xenon

lamp (λ > 420 nm). During the test, 10 mg of the photocatalyst was dispersed in 100 mL TC solution (100 mg/L) and sonicated for 20 min in the dark environment to achieve adsorption-desorption equilibrium. Subsequently, the solution was exposed to visible light for photodegradation experiments. During the process, 4 mL of the liquid was extracted at -10, 0, 10, 20, 30, 40, 50, and 60 min, and the supernatant was centrifuged and analyzed for the concentration of TC by UV-Vis diffuse reflectance spectra. The characteristic absorption wavelength of TC was 357 nm, and a quasi-primary kinetic model was used to determine the rate of degradation of TC during the 60-minute reaction cycle constant.

## 3. Experimental results and discussion

### 3.1 Catalyst morphology and structure characterization

The morphology and structure of CN and cyano-UCN 4:14 were explored by TEM, and it can be seen from Fig. 1(a-b) that CN exhibits severe layer-to-layer stacking because of its smaller lamellar size and larger surface energy. While cyano-UCN 4:14 exhibits ultrathin nanostructures, in which the stacking and curling between layers is greatly suppressed, and the surface area of layer is effectively increased. Literature reports confirm that the ultrathin nanosheet structure can effectively shorten the carrier transport path, while providing more active sites for photocatalytic reactions.[21] HR-TEM images exhibited in Fig. 1(c-d) exhibit that the two materials belong to the amorphous structure. Isothermal adsorption-desorption plots in Fig. S1 indicate that g-$C_3N_4$ has a typical Langmuir IV adsorption-desorption curve, and its specific surface area of cyano-UCN is 173.89 $m^2g^{-1}$, which is 27 times higher than that of CN (6.44 $m^2g^{-1}$). The BET results further validate the ultrathin nanosheet g-$C_3N_4$ is achieved by salt-assisted heat treatment method. The inner reason may lie in the fact that the adding of NaCl forms a liquid or molten state environment at high temperatures. It may play a spatial barrier role during the polymerization process of the g-$C_3N_4$ precursor, thereby facilitating the formation of ultrathin nanosheet structure.

The surface chemical states of CN and cyano-UCN 4:14 can be observed by XPS characterization. The XPS fitting curves of C 1s, N 1s, and O 1s are depicted in Fig. 2(a-d) and Fig. S2. In Fig. 2a, the C 1s peak located at 284.80 eV and288.31 eV represent the exogenous carbon and the $sp^2$ hybridized carbon of N-C=N in CN, respectively. The peak located at 286.26 eV represents the cyano group (C≡N), which is originated from an inevitable incomplete polycondensation reaction. By comparing the fitting peaks of C≡N for CN and cyano-UCN 4:14 in Fig. 2a and b, it is obvious to find that the peak area of cyano group for cyano-UCN 4:14 is larger than that of CN. Thus, it confirms the successful introduction of cyano groups in g-$C_3N_4$ framework through salt-assisted thermal treatment method. The N 1s spectra are displayed in Fig. 2c and d. In which the peak at 398.68 eV is originated from the $sp^2$-bonded nitrogen (C=N-C) in the tris-s-triazine ring. The peak at 399.46 eV is attributed to the terminal amino functional group (-$NH_x$), and the peak at 401.11 eV represents the bridging nitrogen atom (N-$(C)^3$).[22-24] It is surprising to find that the peak of -$NH_x$ incyano-UCN 4:14 is almost disappeared.

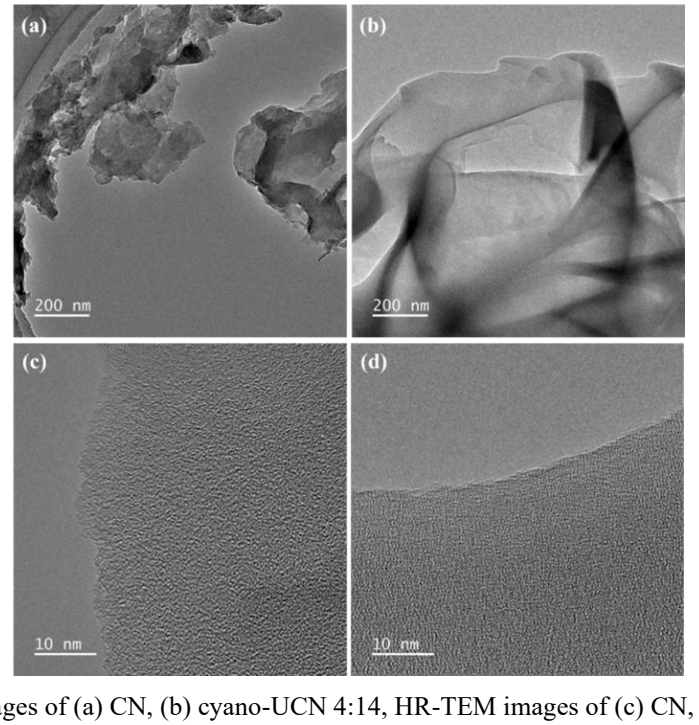


**Fig. 1:** TEM images of (a) CN, (b) cyano-UCN 4:14, HR-TEM images of (c) CN, (d) cyano-UCN 4:14.

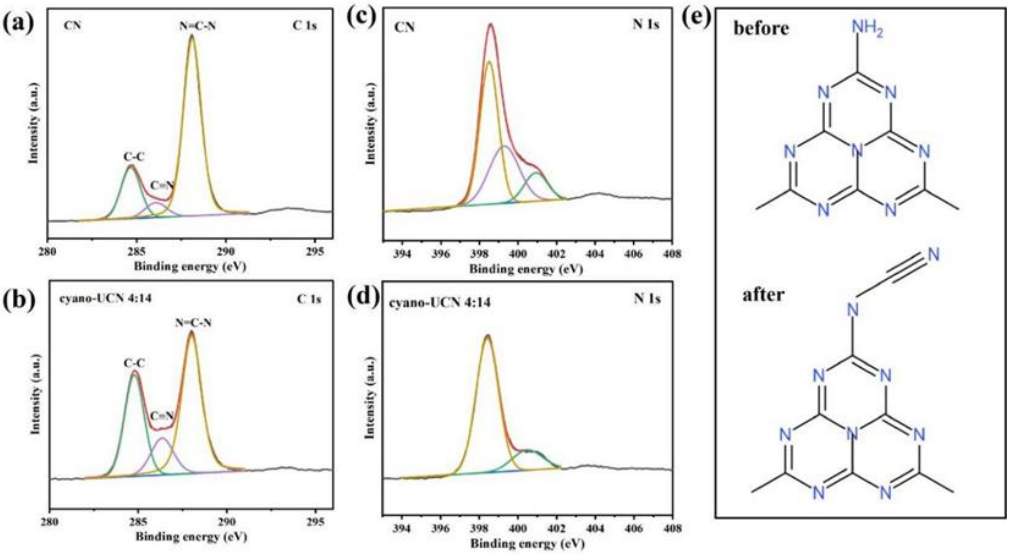


**Fig. 2:** XPS spectra of (a) C 1s, (c) N 1s of CN and (b) C 1s, (d)N 1s of cyano-UCN 4:14, (e) the molecular structure of pristine g-$C_3N_4$ and cyano-modified g-$C_3N_4$.

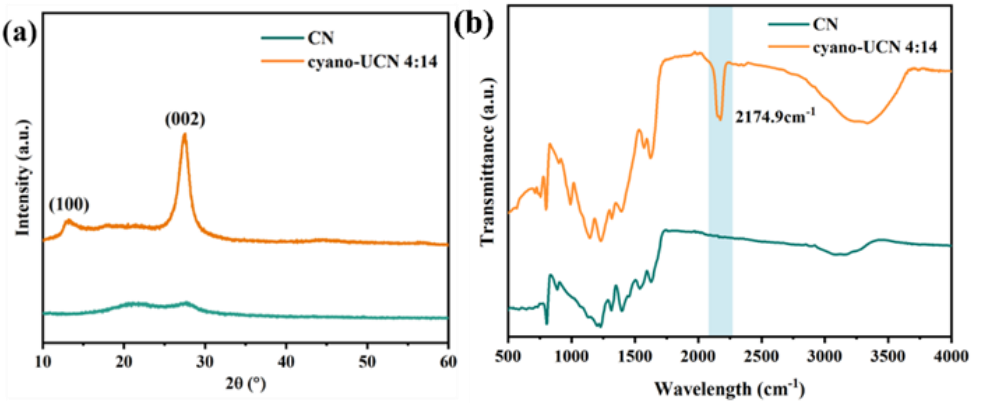


**Fig. 3:** (a) XRD pattern and (b) FT-IR spectrum of CN, cyano-CN 4:14.

Thus, it is reasonably to deduced that the -NHx is replaced by N-C≡N as shown in Fig. 2e. Fig. S2a-b depicts the XPS fitting peaks of O 1s. It is obvious to find that only a single peak appears in CN, which represents the C-O group. While the spectrum of cyano-UCN 4:14 exhibits two peaks, which are caused by the C-O group and the O-H on the adsorbed water molecules, respectively. According to the literature, the O-H peak is caused by water molecules adsorbed on the materials surface during synthesis or storage.[25]

The compositional information of the samples is analyzed by FT-IR and XRD. It can be seen from the XRD spectra in Fig. 3a that CN possess the typical characteristic peaks of g-$C_3N_4$. The former peaks located near 13° attributed to the (100) facet of the triazine-s-triazine unit within the CN unit layer, and the latter peaks located at 27.5° representing the (002) facet of the interplanar stacking. Comparison of the diffraction peaks for the two materials, it is revealed that the (002) peak of cyano-UCN 4:14 shifts from 27.49° to 27.77°. According to the equation of $d=\lambda/2\sin\theta$, it is reasonably to infer that the layer distance between the two neighboring unitary layers of cyano-UCN 4:14 is narrower, which might be attributed to that the strong end-groups of cyano enhance the interactions between the neighboring layers.[26] By contrast, no diffraction peak of (100) is detected, which suggests that the reaction of NaCl with dicyandiamide during thermal polymerization reduces the long-range ordering within the structural facets.[27-28] The FT-IR spectra are shown in Fig. 3b, and absorption peaks located at 810 $cm^{-1}$ originates from the out-of-plane bending vibration of the triazine-s-triazine ring in the CN structure. The peaks in the range of 1200-1700 $cm^{-1}$ belong to the stretching vibrations of aromatic C-N or C=N heterocycles.[29] The broad peaks in the range of 3000-3400 $cm^{-1}$ correspond to the stretching vibrations of the -N-H bond in the amino group and the hydrogen bonding interactions of adsorbed water molecules.[30] It is obvious to find that the vibration peak in 3000-3400 $cm^{-1}$ of cyano-UCN 4:14 is lower

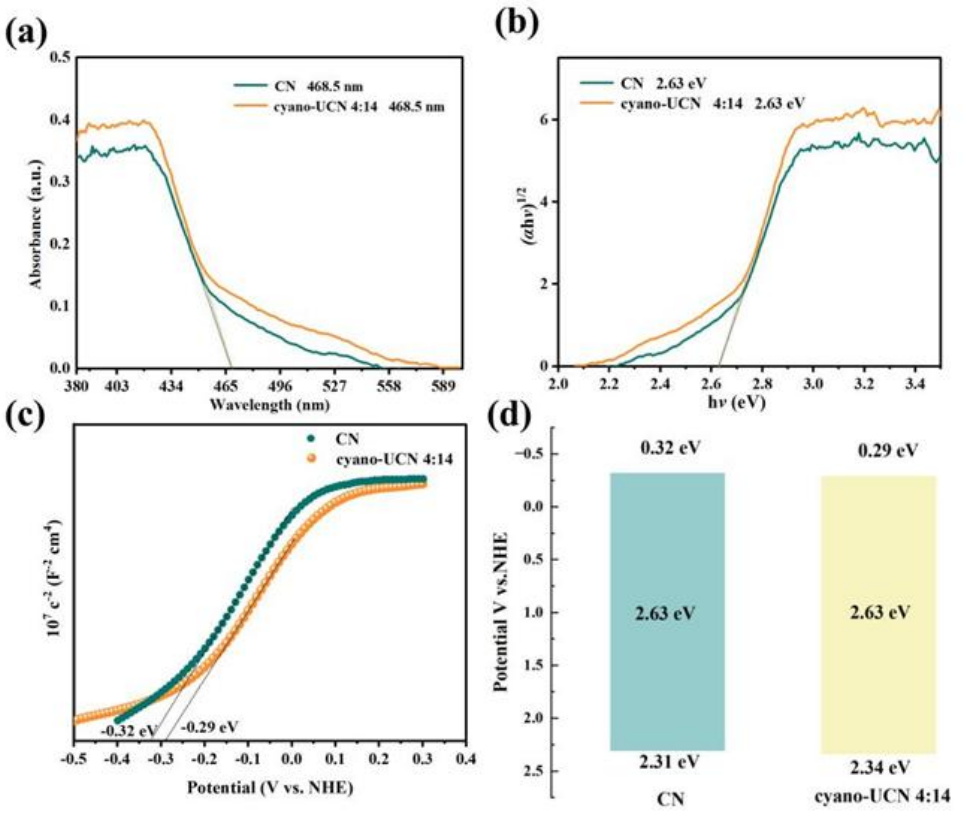


**Fig. 4:** (a) UV-Vis absorption spectra, (b) Kubelka-Munk plot curves, (c) M-S plots, and (d) energy band energy maps of CN, cyano-UCN 4:14.

than that of CN, which might be attributed to the replacement of -N-H bond to -N-C≡N.[31] In addition, unlike CN, a distinct characteristic peak at 2177.7 $cm^{-1}$ is appeared for cyano-UCN 4:14, which represents the stretching vibration of C≡N.[32] The successfully introduction of cyano in the g-$C_3N_4$ framework is proved again, which is originated from the incomplete polymerization and/or partial decomposition of the triazine-s-triazine unit during synthesis induced by NaCl.[33]

### 3.2 Optical properties and photocatalytic degradation efficiency

UV-Vis absorption spectra and Kubelka-Munk plot curves are depicted in Fig. 4a-b.[34] The light absorption properties of CN and cyano-UCN 4:14 can be understood by UV-Vis DRS as shown in Fig. 4a. Both CN and cyano-UCN 4:14 exhibit typical semiconductor light absorption properties with the absorption edge located at 468.5 nm. It is obviously seen that a higher light absorption intensity is achieved for cyano-UCN 4:14 in the visible light absorption range. Since the nanostructuring of g-$C_3N_4$ usually leads to an increase in the band gap due to quantum size effect,[35] the enhancement of cyano-UCN light absorption can be attributed to cyano groups. The bandgap value ($E_g$) of both samples is about 2.63 eV as calculated by the K-M formula (Fig. 4b). As the M-S plots show in Fig. 4c, the values of conduction band ($E_{CB}$) of CN and cyano-UCN 4:14 are -0.32 eV and -0.29 eV, respectively. According to the formula of $E_g=E_{CB}+E_{VB}$, the energy of valence band ($E_{VB}$) are calculated to be 2.31 eV and 2.34 eV, respectively. Based on above, the energy band diagrams of CN and cyano-UCN 4:14 are depicted in Fig. 4d. It is obvious to find that the $E_{VB}$ of cyano-UCN 4:14 is higher than that of CN, indicating a stronger oxidizing ability of cyano-modified samples. Therefore, water molecules can be oxidized into hydroxyl radicals by holes, and then tetracycline can be effectively oxidized and degraded.[36]

The photocatalytic performance of the materials was evalueded by the degradation efficiency of TC under 300 W xenon lamp (λ>420 nm) irradiation. The photocatalytic degradation efficiency of CN and all cyano-modified samples is shown by Fig. 5a. In the absence of catalyst addition or light irradiation, there is hardly any degradation efficiency, which proves that the pollution cannot degrade without photocatalytic, and the degradation efficiency of TC under dark conditions is poor. It is obvious seen from Fig. 5a that CN has almost no TC degradation ability. Surprisingly, the TC degradation performance of cyano-UCN in different ratio is effectively improved. Among them, the photodegradation efficiency of TC by cyano-UCN 4:14 reaches 98.96% after 60

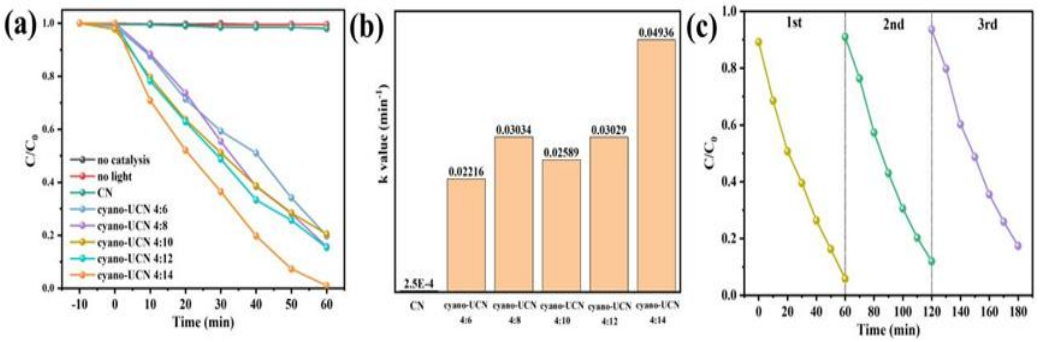


**Fig. 5:** (a) TC degradation efficiencies for different samples, (b) comparison of photocatalytic degradation kinetics of k value, (c) cycling performance of cyano-UCN 4:14 in 3 h.

min of continuous visible light irradiation, which is much higher than that of cyano-UCN 4:12 (84.62%), cyano-UCN 4:10 (79.55%), cyano-UCN 4:8 (84.32%), and cyano-UCN 4:6 (80.22%). In addition, the corresponding kinetic rate constant (k) is calculated and depicted in Fig. 5b according to the following equation: $-\ln(C/C_0)=kt$, where $C_0$ and C represent the initial light absorption intensity of TC and the light absorption intensity of TC at t min, respectively. As can be seen from Fig. 5b and Fig. S3, the k value of cyano-UCN 4:14 reaches 0.04936 $min^{-1}$, which is 1.63 times, 1.91 times, 1.63 times and 2.23 times that of cyano-UCN 4:12 (k =0.03029 $min^{-1}$), cyano-UCN 4:10 (k = 0.02589 $min^{-1}$), cyano-UCN 4:8 (k = 0.03034 $min^{-1}$) and cyano-UCN 4:6 (k = 0.02216 $min^{-1}$), respectively. The cycling perfomance is exhibited in Fig. 5c, in which the TC removal rate still remain 82.6% after 3 h visible light irradiation. The degradation efficiency is retained 87.7% in three cycles. Compared with the relevant literature shown in Table S1, the TC degradation performance of cyano-UCN 4:14 in this study is remarkable. Considering the ultra-low concentration of the catalyst (0.1 g/L) and the ultra-high concentration of TC (100 mg/L) used in the experiment, the TC degradation performance in this study exceeds the performance reported in current literatures and is in a leading position in the industry.

### 3.3 Research on photocatalytic mechanism

Optical current density response (I-T), PL and electrochemical impedance spectroscopy (EIS) are effective methods to study the separation efficiency of photo-excited electron-hole pairs. Fig. 6a exhibits that the I-T response of cyano-UCN 4:14 is significantly higher than that of CN, demonstrating a promoted carrier mobility efficiency for cyano-UCN 4:14 under visible light irradiation.[37] The fluorescence intensity of PL spectra in Fig. 6b reflects the exciton recombination

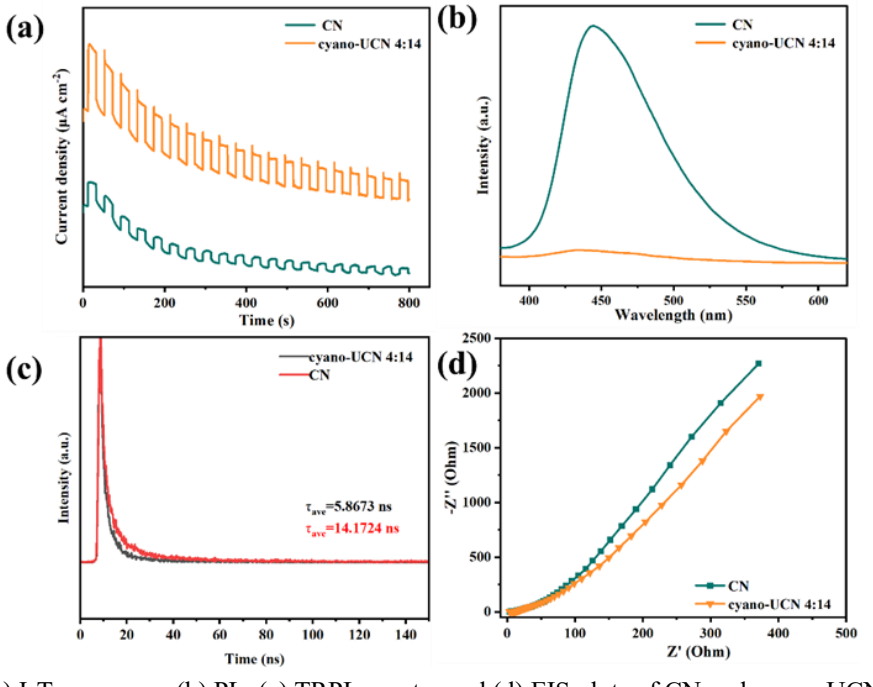


**Fig. 6:** (a) I-T responses, (b) PL, (c) TRPL spectra and (d) EIS plots of CN and cyano-UCN 4:14.

efficiency. The intensity of cyano-UCN 4:14 is substantially weakened relative to the peak intensity of CN, implying that the exciton combination rate of cyano-UCN 4:14 is significantly reduced. This phenomenon occurs because the highly electron-withdrawing effect of cyano in the cyano-UCN network effectively modulates the electronic structure of g-$C_3N_4$ and therefore attracts electrons to form locally polarized sites, thus reducing the combination of electron-hole.[38] The TRPL spectra were conducted to reveal the behavior of excited-state carriers in materials (Fig. 6c). The $\tau_{ave}$ of cyano-UCN 4:14 (5.8673 ns) is shorter than that of CN (14.1724 ns), indicating that electron-hole separation and transfer are effectively enhanced, demonstrating that the ultra-thin nanosheet structure can effectively shorten the carrier transport path. In addition, EIS plots in Fig. 6d show that the semicircular radius of cyano-UCN 4；14 is significantly lower than that of CN, suggesting that cyano-modified ultrathin g-$C_3N_4$ has more efficient photogenerated electron-hole separation ability. The enhanced carrier separation and migration ability is attributed to the ultrathin 2D lamellar structure that effectively shortens the carrier migration path, and its enlarged surface area can provide more active sites for charge carriers, thus prompting more carriers to migrate to the surface active sites to participate in the TC degradation process.[39]

To further investigate the main active substances in the photocatalytic degradation of TC, tert-butanol (BuOH), 2,2,6,6 tetramethylpiperidine oxide (TEMPO), and L-tryptophan (L-trp) were used as scavengers for free radical trapping experiments to remove hydroxyl radicals (·OH), superoxide radicals ($\cdot O_2^-$) and linear oxide radicals ($^1O_2$). As shown in Fig. 7a, the degradation efficiencies after the addition of BuOH, TEMPO, and L-trp are about 82.40%, 90.50%, and 62.39%, respectively. It indicates that ·OH, $^1O_2$ are the most effective reactive oxygen species and $O_2^-$ is the less effective reactive oxygen species in photocatalytic degradation. In addition, the reactive oxygen species were also detected by ESR after 5 min light radiation. In the experiments, 5,5-dimethyl-1-pyrroline-n-oxide (DMPO) was employed to capture OH in water, $\cdot O_2^-$ was detected in methanol, and TEMPO was used to capture $^1O_2$.[40,41] It is obvious to find the characteristic peak of all reactive oxygen species in Fig. 7b.

Therefore, the combined radical trapping experiments and ESR spectra analysis label $\cdot O_2^-$, $^1O_2$ and ·OH as the main active substances in the photocatalytic degradation of TC by cyano-UCN 4:14.

To further investigate the TC degradation pathways, LC-MS was used to analyze the TC intermediates during the photocatalytic degradation of cyano-UCN 4:14. The mass spectra of these intermediates are shown in Fig. S4. In this study, the assay infers two possible decomposition pathways as shown in Fig. 8. In pathway I, the intermediate product TC1 (m/z = 394) is generated by reduction reaction, dehydrogenation, deamination and demethylation of TC. TC1 transforms into TC2 (m/z = 309) by ring opening, hydrogenation of the benzene ring, alkylation and hydroxylation. TC2 undergoes dehydrogenation to form TC3 (m/z = 292). In pathway II, TC4 (m/z = 417) is obtained by hydroxylation and demethylation of TC.[42] TC4 undergoes dehydroxylation, benzene ring opening and hydroxylation to yield TC5 (m/z = 349). TC5 undergoes hydrogenation of the benzene ring and decarboxylation to yield TC6 (m/z = 280). These intermediates are further subjected to ring-opening, addition, and oxidation reactions to form TC7-TC12. Finally, these small molecule intermediates were mineralized to $CO_2$ and $H_2O$.

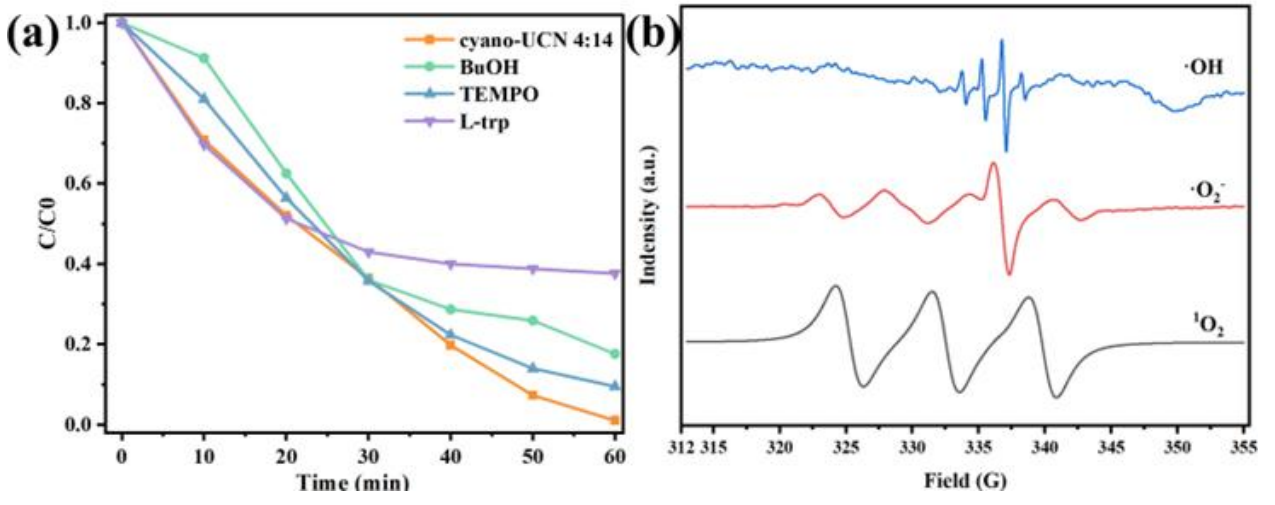


**Fig. 7:** (a) Trapping experiments of active substances during photocatalytic degradation of TC by cyano-UCN 4:14 under visible light irradiation, (b) ESR spectra for the detection of $\cdot O_2^-$, $^1O_2$, and ·OH.

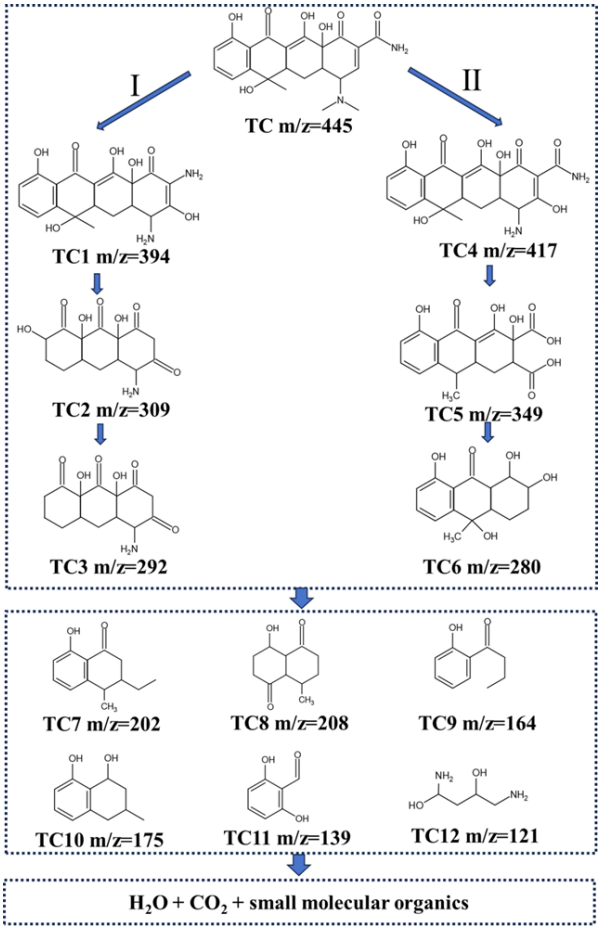


**Fig. 8:** Possible photodegradation pathways of TC by cyano-UCN 4:14.

Based on above, a possible photocatalytic mechanism for the enhancement of the photocatalytic degradation is proposed in this research. Salt-assisted heat treatment method leads to the expansion of g-$C_3N_4$ surface area. The ultrathin 2D structure of cyano-UCN 4:14 leads to an expanded specific surface area, thus shortens the transfer route of charge carriers and effectively enhances the amount of electron and holes migrations to the surface. However, there is still a risk of recombination for the surface electron-hole surfaces. Therefore, cyano groups with strong electrons capture ability grafting are introduced in the framework of g-$C_3N_4$, validly suppressing the recombination efficiency of charge carriers on the surface. Thus, the carriers transfer kinetics is reasonably improved on the cooperation of the ultrathin structure and cyano groups. Furthermore, the cyano-modified ultrathin g-$C_3N_4$ with higher $E_{CB}$ values has higher oxidizing ability in the photo-excited state. Thus the cyano-UCN samples show ultra-high visible-light photocatalytic degradation efficiencies for TC.

## 4. Conclusion

In summary, we employed a simple and efficient salt-assisted thermal treatment method to successfully prepare cyano-modified ultrathin g-$C_3N_4$. The reduction of the layer stacking for g-$C_3N_4$ can effectively shortening the carrier transport paths while providing more abundant activation sites on the surface. Moreover, the strong electron-withdrawing effect of cyano groups can regulate the electronic structure of g-$C_3N_4$ and reduces the recombination efficiency of charge carriers. The synergistic effect of ultrathin structure and cyano groups validly optimizes the carriers transfer kinetics, which results in a significant enhancement of the photocatalytic efficiency of the prepared materials. The results show that the photodegradation efficiency is as high as 98.96% in 1 h with a k value of 0.04936 $min^{-1}$ for high concentration of TC solution (100 mg/L). This research opens up a broad prospect for the application of g-$C_3N_4$ materials in the field of photocatalytic wastewater treatment, and it is summarized as the following two points:

Cyano-modified g-$C_3N_4$ catalysts can be combined with heterojunctions simultaneously to optimize the degradation performance of the material.

This material can be applied to the development of photocatalytic degradation for various pollutants, such as phenols, dyes, and halogenated hydrocarbons.

**Acknowledgments**
This work is supported by the National Natural Science Foundation of China (22203028), the Natural Science Foundation of Hunan Province, China (2023JJ30250, 2023JJ30227, 2023GK2015, 2024JJ5149), Outstanding Youth Project of Hunan Provincial Department of Public Education (23B0468, 24B0459), Student Research and Innovation Program (S202510534182).

**Data availability**
Data will be made available on request.

**Conflict of Interest**
The authors declare that there are no known competing financial interests or personal relationships that could have appeared to influence the work reported in this paper.

**Supporting Information**
Applicable.

**CRediT Statement**
**Xijue Tang** fabricated the samples and did the photocatalysis experiments with the assistance from **Wenqiang Luo** and **Guoyong Wang**. **Huanhuan Zhai** conceived and directed this work. **Shaohui Xiong**, **Hongwei Zhao**, **Xinxiu Cao** and **Danyu Zhang** discussed the results and helped in the organizing the manuscript. **Qingquan Liu** supervised the experiments.

**References**
[1] S Begum, T Begum, N Rahman, R Khan, A review on antibiotic resistance and way of combating antimicrobial resistance, *GSC Biological and Pharmaceutical Sciences*, 2021, **14**, 87-97, doi: 10.30574/gscbps.2021.14.2.0037.
[2] X Chen, Y Ke, Y Zhu, M Xu, C Chen, S Xie, Enrichment of tetracycline-degrading bacterial consortia: Microbial community succession and degradation characteristics and mechanism, *Journal of Hazardous Materials*, 2021, **448**, 130984, doi: 10.1016/j.jhazmat.2023.130984.
[3] Q He, Y Yi, W Shi, P Sun, X Dong, Determination of the key role to affect the piezocatalytic activity of graphitic carbon nitride for tetracycline hydrochloride degradation in water, *Chemosphere*, 2023, **317**, 137828, doi: 10.1016/j.chemosphere.2023.137828.
[4] X Sun, D Jiang, L Zhang, W Wang, Alkaline modified g-$C_3N_4$ photocatalyst for high selective oxide coupling of benzyl alcohol to benzoin, *Applied Catalysis B: Environmental*, 2018, **220**, 553-560, doi: 10.1016/j.apcatb.2017.08.057.
[5] S Guo, Y Tang, Y Xie, C Tian, Q Feng, W Zhou, B Jiang, P-doped tubular g-$C_3N_4$ with surface carbon defects: Universal synthesis and enhanced visible-light photocatalytic hydrogen production, *Applied Catalysis B: Environmental*, 2017, **218**, 664-671, doi: 10.1016/j.apcatb.2017.07.022.
[6] W Zhang, Y Fu, J Wang, X Wang, 3D Hierarchically Porous Graphitic Carbon Nitride Modified Graphene-Pt Hybrid as Efficient Methanol Oxidation Catalysts, *Advanced Materials Interfaces*, 2017, **4**, 1601219, doi: 10.1002/admi.201601219.
[7] W Li, W Zhao, Q Luo, W Xiao, X Wang, Y Shi, J Sun, Integration of $WO_x$/1D $C_3N_4$/2D $C_3N_4$ multi-junction through in-situ "PTA-Mel" ionic microenvironment for efficient aromatic wastes degradation via charge carrier separation improvement, *Chemical Engineering Science*, 2024, **293**, 120007, doi: 10.1016/j.ces.2024.120007.
[8] Z Zhou, H Zeng, L Li, R Tang, C Feng, D Gong, Y Huang, Y Deng, Methyl contributes to the directed phosphorus doping of g-$C_3N_4$: pH-dependent selective reactive oxygen species enable customized degradation of organic pollutants, *Water Research*, 2024, **255**, 121521, doi: 10.1016/j.watres.2024.121521.
[9] L Jiang, X Yuan, Y Pan, J Liang, G Zeng, Z Wu, H Wang, Doping of graphitic carbon nitride for photocatalysis: A review, *Applied Catalysis B: Environmental*, 2017, **217**, 388-406, doi: 10.1016/j.apcatb.2017.06.003.
[10] T Yao, H Wang, X Ji, D Wang, Q Zhang, L Meng, J Shi, X Han, Y Cheng, Introducing Hybrid Defects of Silicon Doping and Oxygen Vacancies into MOF-Derived $TiO_{2-X}$ @Carbon Nanotablets Toward High-Performance Sodium-Ion Storage, *Small*, 2023, **19**, e2302831, doi: 10.1002/smll.202302831.
[11] Z Bai, C Wang, J Pei, J He, J Liu, Constructing Z-scheme heterojunction of AC@g-$C_3N_4$/$MnO_x$ for effective removal of acetaldehyde in building environment, *Building and Environment*, 2025, **280**, 113137, doi: 10.1016/j.buildenv.2025.113137.
[12] W Wang, J Fang, S Shao, M Lai, C Lu, Compact and uniform $TiO_2$@g-$C_3N_4$ core-shell quantum heterojunction for photocatalytic degradation of tetracycline antibiotics, *Applied Catalysis B: Environmental*, 2017, **217**, 57-64, doi: 10.1016/j.apcatb.2017.05.037.
[13] D He, Y Chen, Y Situ, L Zhong, H Huang, Synthesis of ternary g-$C_3N_4$/Ag/γ-FeOOH photocatalyst: An integrated heterogeneous Fenton-like system for effectively degradation of azo dye methyl orange under visible light, *Applied Surface Science*, 2017, **425**, 862-872, doi: 10.1016/j.apsusc.2017.06.124.
[14] W Hu, J Yu, X Jiang, X Liu, R Jin, Y Lu, L Zhao, Y Wu, Y He, Enhanced photocatalytic activity of g-$C_3N_4$ via modification of NiMoO4 nanorods, *Colloids and Surfaces A: Physicochemical*

*and Engineering Aspects*, 2017, **514**, 98-106, doi: 10.1016/j.colsurfa.2016.11.058.

[15] J Cheng, C Li, Z Yu, H Liu, Efficient photohydrogen production by edge-modified carbon nitride with nonmetallic group, *Journal of Colloid and Interface Science*, 2023, **629**, 739-749, doi: 10.1016/j.jcis.2022.09.121.

[16] L Zeng, Y Zhao, X Jia, Y Jiang, L Huang, Surface oxygenous groups modified graphitic carbon nitride with significant positive shift of valence band for efficient photocatalytic oxidation, *Applied Surface Science*, 2021, **563**, 150070, doi: 10.1016/j.apsusc.2021.150070.

[17] H Yang, S Sun, J Lyu, Q Yang, J Cui, Mechanism insight into triple S-Scheme intermolecular carbon nitride homojunction with robust built-in electric field for highly enhanced photocatalytic hydrogen evolution, *Chemical Engineering Journal*, 2024, **481**, 148297, doi: 10.1016/j.cej.2023.148297.

[18] TVA Hoang, PA Nguyen, EW Shin, Effect of Morphological Modification over g-$C_3N_4$ on Photocatalytic Hydrogen Evolution Performance of g-C3N4-Pt Photocatalysts, *Catalysts*, 2023,**13**, 92, doi: 10.3390/catal13010092.

[19] Y Zheng, Q Ruan, J Ren, X Guo, Y Zhou, B Zhou, Q Xu, Q Fu, S Wang, Y Huang, Plasma- assisted liquid-based growth of g-$C_3N_4$/$Mn_2O_3$ p-n heterojunction with tunable valence band for photoelectrochemical application, *Applied Catalysis B: Environmental*, 2023, **323**, 122170, doi: 10.1016/j.apcatb.2022.122170.

[20] Z Shu, Y Wang, W Wang, J Zhou, T Li, X Liu, Y Tan, Z Zhao, A green one-pot approach for mesoporous g-C3N4 nanosheets with in situ sodium doping for enhanced photocatalytic hydrogen evolution, *International Journal of Hydrogen Energy*, 2019, **44**, 748-756, doi: 10.1016/j.ijhydene.2018.11.025.

[21] T Yang, Y Shao, J Hu, J Qu, X Yang, F Yang, Li C Ming, Ultrathin layered 2D/2D heterojunction of ReS2/high-crystalline g-C3N4 for significantly improved photocatalytic hydrogen evolution, *Chemical Engineering Journal*, 2022, **448**, 137613, doi: 10.1016/j.cej.2022.137613.

[22] Y Xu, Y Gong, H Ren, W Liu, L Niu, C Li, X Liu, In situ structural modification of graphitic carbon nitride by alkali halides and influence on photocatalytic activity, *RSC Advances*, 2017, **7**, 32592-32600, doi: 10.1039/C7RA05555B.

[23] S Cao, Q Huang, B Zhu, J Yu, Trace-level phosphorus and sodium co-doping of g-$C_3N_4$ for enhanced photocatalytic H2 production, *Journal of Power Sources*, 2017, **351**, 151-159, doi: 10.1016/j.jpowsour.2017.03.089.

[24] K Wang, X Wang, H Pan, Y Liu, S Xu, S Cao, In situ fabrication of CDs/g-$C_3N_4$ hybrids with enhanced interface connection via calcination of the precursors for photocatalytic $H_2$ evolution, *International Journal of Hydrogen Energy*, 2018, **43**, 91-99, doi: 10.1016/j.ijhydene.2017.11.003.

[25] Z Shu, Y Wang, W Wang, J Zhou, T Li, X Liu, Y Tan, Z Zhao, A green one-pot approach for mesoporous g-$C_3N_4$ nanosheets with in situ sodium doping for enhanced photocatalytic hydrogen evolution, *International Journal of Hydrogen Energy*, 2019, **44**, 748–756, doi: 10.1016/j.ijhydene.2018.11.025.

[26] B Yang, L Lu, Q Zhang, G Ding, G Liao, M Zhang, X Liu, Rodriguez D, Jia XEnhanced built-in electric fields in alkali metal-doped $C_3N_5$ enable sustainable molecular oxygen activation for water purification, *Chemical Engineering Journal*, 2025, **509**, 161236, doi: 10.1016/j.cej.2025.161236.

[27] L Lin, H Ou, Y Zhang, X Wang, Tri-s-triazine-Based Crystalline Graphitic Carbon Nitrides for Highly Efficient Hydrogen Evolution Photocatalysis, *ACS Catalysis*, 2016, **6**, 3921-3931, doi: 10.1021/acscatal.6b00922.

[28] G Zhang, L Lin, G Li, Y Zhang, A Savateev, S Zafeiratos, X Wang, M Antonietti, Ionothermal Synthesis of Triazine-Heptazine-Based Copolymers with Apparent Quantum Yields of 60 % at 420 nm for Solar Hydrogen Production from “Sea Water.” *Angewandte Chemie International Edition*, 2018, **57**, 9372-9376, doi: 10.1002/anie.201804702.

[29] Q Liang, Z Li, Q Yang, Y Bai, Z Huang, F Kang, Reduced-sized monolayer carbon nitride nanosheets for highly improved photoresponse for cell imaging and photocatalysis, *Science China Materials*, 2017, **60**, 109-118, doi: 10.1007/s40843-016-5131-9.

[30] L Luo, A Zhang, MJ Janik, C Song, X Guo, Facile fabrication of metal-free urchin-like g-$C_3N_4$ with superior photocatalytic activity, *RSC Advances*, 2016, **6**, 94496-94501, doi: 10.1039/C6RA20940H.

[31] J Yuan, X Liu, Y Tang, Y Zeng, L Wang, S Zhang, T Cai, Y Liu, S Luo, Y Pei, C Liu, Positioning cyanamide defects in g-$C_3N_4$: Engineering energy levels and active sites for superior photocatalytic hydrogen evolution, *Applied Catalysis B: Environmental*, 2018, **237**, 24-31, doi: 10.1016/j.apcatb.2018.05.064.

[32] Y Wang, Y Li, W Ju, J Wang, H Yao, L Yao, J Wang, Z Li, Molten salt synthesis of water-dispersible polymeric carbon nitride nanoseaweeds and their application as luminescent probes, *Carbon*, 2016, **102**, 477-486, doi: 10.1016/j.carbon.2016.02.065.

[33] Y Li, H Xu, S Ouyang, D Lu, D Wang, J Ye, In situ surface alkalinized g-$C_3N_4$ toward enhancement of photocatalytic $H_2$ evolution under visible-light irradiation, *Journal of Materials Chemistry A*, 2016, **4**, 2943-2950, doi: 10.1039/C5TA05128B.

[34] D Liu, C Zhang, J Shi, L Li, W Liu, M Liu, J Su, J Liu, L Guo, Constructing asymmetric dual active sites of Ag single atoms and nitrogen defects on carbon nitride for enhanced photocatalytic $H_2O_2$ production. *Journal of Materials Science & Technology*, 2025, **223**, 56-65, doi: 10.1016/j.jmst.2024.09.048.

[35] Z Shu, C Xie, J Zhou, T Li, Y Chen, W Wang, Y Tan, Z Zhao, Nanoporous g-$C_3N_4$ nanosheets: Facile synthesis and excellent

visible-light photocatalytic H2 evolution performance, *Journal of Alloys and Compounds*, 2018, **747**, 140-148, doi: 10.1016/j.jallcom.2018.03.019.
[36] L Liang, L Shi, F Wang, P Yan, Y Cong, L Yao, Z Yang, Qi W, g-$C_3N_4$ nano-fragments as highly efficient hydrogen evolution photocatalysts: Boosting effect of nitrogen vacancy, *Applied Catalysis A: General*, 2020, **599**, 117618, doi: 10.1016/j.apcata.2020.117618.
[37] Z Chen, S Lu, Q Wu, F He, N Zhao, C He, C Shi, Salt-assisted synthesis of 3D open porous g-C3N4 decorated with cyano groups for photocatalytic hydrogen evolution, *Nanoscale*, 2018, **10**, 3008-3013, doi: 10.1039/C7NR05927B.
[38] K Li, L Bao, S Cao, Y Xue, S Yan, H Gao, Template-Assisted Surface Hydrophilicity of Graphitic Carbon Nitride for Enhanced Photocatalytic H2 Evolution, *ACS Applied Energy Materials*, 2021, **4**, 12965-12973, doi: 10.1021/acsaem.1c02602.
[39] X Liang, Y Zhang, D Li, B Wen, D Jiang, M Chen, 2D/2D BiOCl/$K^+Ca_2Nb_3O_{10}^-$ heterostructure with Z-scheme charge carrier transfer pathways for tetracycline degradation under simulated solar light, *Applied Surface Science*, 2019, **466**, 863-873, doi: 10.1016/j.apsusc.2018.10.057.
[40] Y Sun, L Shen, Q Qin, L Jiang, Y Su, Y Wang, L Xia, S Lin, W Yao, Q Wu, Q Xu, Enhanced reactive oxygen species via in situ producing $H_2O_2$ and synchronous catalytic conversion at stable modified copper foam cathode for efficient high-concentration organic wastewater treatment and simultaneous electricity generation, *Chemosphere,* 2022, **291**, 132911, doi: 10.1016/j.chemosphere.2021.132911
[41] H Liu, X Wang, Z Lan, Cryogenic ball milling synthesis of $Ag_3PO_4$/h-BN nanoparticles with increased performance for photocatalytic oxygen evolution reaction, *Ceramics International*, 2019, **45**, 16682-16687, doi: 10.1016/j.ceramint.2019.05.117
[42] L Liu, M Yu, Y Li, C Han, G Ding, S Liu, Y Xie, J Liu, Microwave (MW)-assisted design of cobalt anchored 2D graphene-like carbon nanosheets (Co@GCNs) as peroxymonosulfate activator for tetracycline degradation and insight into the catalytic mechanism, *Separation and Purification Technology*, 2022, **295**, 121358, doi: 10.1016/j.seppur.2022.121358.